UNIVERSITY OF BIRMINGHAM
University of Birmingham Research at Birmingham

A discrete multi-physics model to simulate fluid structure interaction and breakage of capsules filled with liquid under coaxial load

Ruiz-Riancho, Ignacio Nilo ; Alexiadis, Alessio; Zhang, Zhibing; Garcia Hernandez, Alvaro

DOI:
10.3390/pr9020354

License:
Creative Commons: Attribution (CC BY)

Document Version
Publisher's PDF, also known as Version of record

Citation for published version (Harvard):
Ruiz-Riancho, IN, Alexiadis, A, Zhang, Z & Garcia Hernandez, A 2021, 'A discrete multi-physics model to simulate fluid structure interaction and breakage of capsules filled with liquid under coaxial load', *Processes*, vol. 9, no. 2, 354. https://doi.org/10.3390/pr9020354

Link to publication on Research at Birmingham portal

General rights
Unless a licence is specified above, all rights (including copyright and moral rights) in this document are retained by the authors and/or the copyright holders. The express permission of the copyright holder must be obtained for any use of this material other than for purposes permitted by law.

•Users may freely distribute the URL that is used to identify this publication.
•Users may download and/or print one copy of the publication from the University of Birmingham research portal for the purpose of private study or non-commercial research.
•User may use extracts from the document in line with the concept of 'fair dealing' under the Copyright, Designs and Patents Act 1988 (?)
•Users may not further distribute the material nor use it for the purposes of commercial gain.

Where a licence is displayed above, please note the terms and conditions of the licence govern your use of this document.

When citing, please reference the published version.

Take down policy
While the University of Birmingham exercises care and attention in making items available there are rare occasions when an item has been uploaded in error or has been deemed to be commercially or otherwise sensitive.

If you believe that this is the case for this document, please contact UBIRA@lists.bham.ac.uk providing details and we will remove access to the work immediately and investigate.

Download date: 20. Apr. 2024

processes

MDPI

Article

A Discrete Multi-Physics Model to Simulate Fluid Structure Interaction and Breakage of Capsules Filled with Liquid under Coaxial Load

Ignacio Nilo Ruiz-Riancho [1], Alessio Alexiadis [2], Zhibing Zhang [2] and Alvaro Garcia Hernandez [1,*]

[1] Nottingham Transportation Engineering Centre, Department of Civil Engineering, University of Nottingham, Nottingham NG7 2RD, UK; niloruizriancho@gmail.com
[2] School of Chemical Engineering, University of Birmingham, Birmingham B15 2TT, UK; A.Alexiadis@bham.ac.uk (A.A.); Z.Zhang@bham.ac.uk (Z.Z.)
* Correspondence: alvaro.garcia@nottingham.ac.uk; Tel.: +44-(0)-0115-95-13914

Abstract: This paper investigated the mechanical response (including breakage and release of the internal liquid) of single core–shell capsules under compression by means of discrete multi-physics. The model combined Smoothed Particle Hydrodynamics for modelling the fluid and the Lattice Spring Model for the elastic membrane. Thanks to the meshless nature of discrete multi-physics, the model can easily account for the fracture of the capsule's shell and the interactions between the internal liquid and the solid shell. The simulations replicated a parallel plate compression test of a single core–shell capsule. The inputs of the model were the size of the capsule, the thickness of the shell, the geometry of the internal structure, the Young's modulus of the shell material, and the fluid's density and viscosity. The outputs of the model were the fracture type, the maximum force needed for the fracture, and the force–displacement curve. The data were validated by reproducing equivalent experimental tests in the laboratory. The simulations accurately reproduced the breakage of capsules with different mechanical properties. The proposed model can be used as a tool for designing capsules that, under stress, break and release their internal liquid at a specific time.

Keywords: capsule; discrete multi-physics; breakable solids simulation; Smoothed Particle Hydrodynamics; Lattice Spring Model

check for updates

Citation: Ruiz-Riancho, I.N.; Alexiadis, A.; Zhang, Z.; Garcia Hernandez, A. A Discrete Multi-Physics Model to Simulate Fluid Structure Interaction and Breakage of Capsules Filled with Liquid under Coaxial Load. *Processes* **2021**, *9*, 354. https://doi.org/10.3390/pr9020354

Academic Editor: Amir Tabakovic

Received: 19 December 2020
Accepted: 8 February 2021
Published: 14 February 2021

Publisher's Note: MDPI stays neutral with regard to jurisdictional claims in published maps and institutional affiliations.

Copyright: © 2021 by the authors. Licensee MDPI, Basel, Switzerland. This article is an open access article distributed under the terms and conditions of the Creative Commons Attribution (CC BY) license (https://creativecommons.org/licenses/by/4.0/).

1. Introduction

A capsule is a solid material enclosing an active substance, often in liquid form. The internal structure of the capsules can vary significantly depending on the encapsulation method and the materials used [1–3]. It can have a simple single-core shell [4], a multicore shell, or a porous structure where the liquid is trapped [5]. Often, the purpose of the capsule is to ensure a controlled release of the liquid inside. With this aim, they are widely used in a variety of fields [6], including cosmetics [7], food [8], textiles [9], pharmacy [10], agriculture [11], and, more recently, for self-healing materials such as self-repairing concrete [12] or asphalt [13,14].

Mechanical characterisation is essential to the design of capsules for a timely release of an active substance [15]. It provides information about material parameters such as the Young's modulus and the stress-strain relationship that are key factors in designing capsules fit for their intended application. Currently, capsules are designed for end-use applications by trial and error. Computer simulations have the potential to significantly accelerate their design by providing a method for predicting the behaviour of the capsule in advance.

Conventional modelling techniques like the Finite Element Method (FEM) can be used to calculate stress in shells [16], but they are less effective when the simulation includes the fracture of the shell. Modelling fluid–solid interactions, occurring after the fracture

of the shell and the consequent release of the fluid, is another main challenge. This issue could be solved by coupling FEM with Smoothed Particle Hydrodynamics (SPH) [17], but this method cannot accurately reproduce the fracture of the shell. Other computational techniques, such as Computational Fluid Dynamics (CFD), Lattice–Boltzmann (LB), and Boundary Integral Methods (BIMs), have been used for simulating solid–fluid flows. However, none of them can simulate breakable solids accurately. Recently, a mesh-free Discrete Multi-Physics (DMP) approach has been implemented to simulate the interactions between fluid and solid particles [18,19]. DMP is based on a particle framework that couples different particle models: SPH to simulate the hydrodynamics of liquid, and the Lattice Spring Model (LSM) to simulate a solid (including high deformations and fracture). These methods share a common particle-based paradigm and, therefore, are easy to couple together. This approach has been validated for a variety of fluid–solid problems. Some examples are the hydrodynamics in the colon [20], motile cilia in the lungs [21], emboli in flexible venous valves [22], phase-change in circular pipes [23], and the deformation and rupture of nucleated cells under shear flows [24].

In this paper, DMP was used to simulate a 3D elastic core–shell capsule breaking under compression and releasing its internal liquid into the environment. To the best of our knowledge, this is the first model capable of simulating this phenomenon. The proposed model is an extension of [24], but, in this case, rupture occurs by direct compression of the capsule rather than as a result of shear flow. The computational results were validated by comparing the type of fracture of the capsule and the force/displacement relationship with experimental data for elastic core–shell capsules available in the literature [25]. DMP can effectively reproduce the deformation and the fracture of the capsule. The model was used to study the influence of the shell's Young's modulus and thickness on the force/displacement relationship and on the type of fracture to show how the proposed model could have a significant impact on the design of capsules [26].

2. Methodology

2.1. Modelling Approach

The version of DMP used in this paper (Figure 1) couples SPH and the LSM. SPH was used to model the fluid, and LSM was used for the solid. Details on these models and how they were coupled together are given in this section.

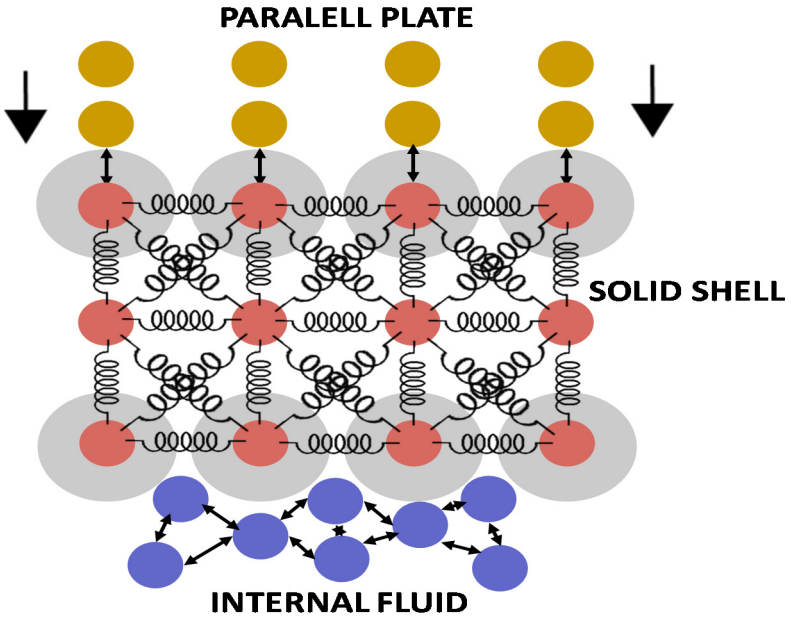

Figure 1. Particle representation and interactions among the computational particles.

2.1.1. Smoothed Particle Hydrodynamics (SPH)

Here, only a very general introduction to SPH is given; for additional details, see [27]. The general idea of SPH is to approximate a partial differential equation over a group of movable computational particles that are not collocated over a grid or a mesh [28]. Each particle has an associated mass, momentum, and energy and the motion of the particle is calculated by integrating Newton's second law. Particle properties such as density, velocity, energy per unit of mass, pressure, or heat flux are obtained by interpolating neighbouring particles by means of:

$$f(\mathbf{r}) \approx \iiint f\left(\mathbf{r}^{'}\right) W\left(\mathbf{r}-\mathbf{r}^{'}, h\right) dr' \tag{1}$$

where $f(\mathbf{r})$ is a generic property defined over the volume, $\mathbf{r}$ is the position vector where the property is measured, W is the so-called Kernel function, and h is a smoothing length [27]. We used the Lucy kernel [29]. The Navier–Stokes equation, for instance, can be discretised over a series of computational particles, obtaining:

$$m_i \frac{dv_i}{dt} = \sum_j m_i m_j \left(\frac{P_i}{\rho_i^2} + \frac{P_j}{\rho_j^2} + \sqcap_{i,j} \right) \nabla_j W_{i,j} + \sum F_E \tag{2}$$

where P is the pressure, t represents time, v is the velocity, m is the mass, ρ is the density associated with particles i and j, and F_E refers to the external forces acting on the fluid (e.g., gravity). The viscosity term ($\sqcap$) used in this study is defined in [30]. Equation (2) requires an equation of state that relates density and pressure. In this work, we used Tait's equation [31]:

$$P(\rho) = \frac{c_0 \rho_0}{7} \left[\left(\frac{\rho}{\rho_0} \right)^7 - 1 \right] \tag{3}$$

where c_0 is a reference speed of sound and ρ_0 is a reference density. To ensure weak compressibility, c_0 was chosen to be at least 10 times larger than the highest fluid velocity.

Π_{ij} in Equation (2) introduces the viscosity tensor; here, we used the so-called artificial viscosity [30], defined as:

$$\Pi_{ij} = -\alpha h \frac{c_0}{\rho_{ij}} \frac{v_{ij} r_{ij}}{r_{ij}^2 + bh^2} \tag{4}$$

where $v_{ij} = v_\mathrm{j} - v_\mathrm{i}$ and $\rho_{ij} = \rho_j + \rho_i$. The dimensionless parameters α and b ensure the stability of the simulation. In our case, b = 0.01, while:

$$\alpha = \frac{8v}{hc_0} \tag{5}$$

where ν is the kinematic viscosity. At each time step, the local density is updated according to the partition of unity equation [30]:

$$\rho_i = \sum_j m_j W_{i,j} \tag{6}$$

2.1.2. Lattice Spring Model (LSM)

The LSM was used to model the shell of the capsule. Here, only a very general introduction to LSM is given; for additional details see [32]. The computational particles that constitute the solid shell are linked together by spring-like bonds and their trajectories calculated with the Newtonian equations of motion:

$$m_i \frac{d^2 r_i}{dt^2} = -\frac{\partial}{\partial r} U_{tot}(r_1, r_2, \ldots r_N) + \sum F_E \tag{7}$$

where U_{tot} is the potential used to model the bonds between interconnected particles. In this study, linear spring was used, which corresponds to the harmonic potential:

$$U_{bond} = k_b(r - r_0)^2 \tag{8}$$

where r_0 is the equilibrium distance and k_b is the Hookean constant. The Young's modulus of the materials relates to k_b, as explained in Section 2.3.

Equation (8) represents the forces that maintain two particles at a specific distance (r_0). The distribution of the shell's computational particles is determined by defining a quadratic mesh (see Figure 1) over an empty sphere with external diameter 3.1×10^{-5} m and an internal diameter of 2.6×10^{-5} m. Nearest neighbour particles and next-nearest neighbour particles are linked with computational springs. Breakage is simulated assuming that, if the distance between two particles exceeds a maximal value (r_{max}), the bond is broken and the two particles separated (Figure 2).

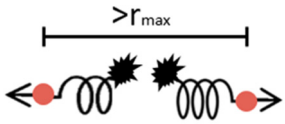

Figure 2. Representation of two computed particle bonds breaking.

How k_b and $r_{\max}$ are calibrated to reproduce the capsule mechanical properties is discussed later on.

2.1.3. Coupling the Two Models

Besides the interaction between two liquid particles (model with SPH) and two solid particles (model with LSM), the model also requires specifying the interaction between liquid and solid particles that occurs at the solid–liquid interface. Here, only a general introduction to coupling SPH and LSM is given; for more details, see [33]. In continuum mechanics, three conditions must be satisfied:

$$\left(\frac{\partial}{\partial t}\mathbf{u} - \mathbf{v}\right) \cdot \mathbf{n} = 0 \ (no\ penetration\ condition) \tag{9}$$

$$\left(\frac{\partial}{\partial t}\mathbf{u} - \mathbf{v}\right) \times \mathbf{n} = 0 \ (no\ slip\ condition) \tag{10}$$

$$\sigma_s \cdot \mathbf{n} = \sigma_f \cdot (-\mathbf{n}) \text{ (continuity of stresses condition)} \tag{11}$$

where $\mathbf{n}$ is the vector normal to the boundary, $\mathbf{u}$ is the displacement of the solid, $\mathbf{v}$ is the velocity of the liquid, and σ_s is the stress tensor in the solid and σ_f in the fluid.

The advantage of using a particle method is that we only solve the Newton equation of motion for every particle. The only difference is in the force acting on the particle. Equations (9)–(11) are no exceptions. They do not need a special treatment, but only forces that replicate the effect of the boundary conditions. For Equation (9), this is achieved by using the repulsive potential of the type:

$$E_r = \epsilon \left[\left(\frac{\sigma}{r}\right)^a - \left(\frac{\sigma}{r}\right)^b \right] r < \sigma \tag{12}$$

where the constants ϵ, σ, a, and b are given in Table 1. This repulsion force does not influence the simulation itself. It is only used to avoid particle compenetrating and its parameters are determined to achieve this goal without requiring a smaller time step. The cut-off $r < \sigma$ in Equation (12) ensures that, when the particles are not in contact, the force is zero. The parameters in Equation (9) were chosen by trial and error to guarantee no penetration without decreasing the timestep. If the repulsion potential is too weak, fluid

will penetrate inside the solid; if it is too strong, the simulation will require small timesteps to remain stable.

Table 1. Parameters needed for Discrete Multi-Physics simulation.

SPH	
Number of SPH fluid particles	5731
Mass of each particle, m	2.7×10^{-15} kg
Initial distance among particles, dL	1.24×10^{-6} m
Smoothing length, h	1.1·dL
Artificial sound speed, c_0	1.1 m s^{-1}
Density, ρ_0	900 kg m^{-3}
Viscosity, μ_0	0.001 Pa·s
LSM	
Number of particles (shell)	5604
Mass of each particle	2.7×10^{-15} kg
Hookean coefficient, kb	4.6 N m^{-1}
Maximum distance for fracture, r_{max}	1.2 r_0
Shell thickness, t_0	2.5×10^{-6} m
Capsule diameter	31×10^{-6} m
BOUNDARIES	
Repulsive potential constant,ϵ	5×10^{-15} J
Repulsive radius, σ	1.1·dL
Repulsive coefficient, a	1
Repulsive coefficient, b	0

No-slip conditions are modelled by superimposing virtual fluid particles above the solid particles at the interface, providing zero relative velocity at the solid–liquid boundary for the liquid particles that interact with the interface. Finally, in particle methods, the continuity-of-stress is automatically satisfied (it is a consequence of the law of action–reaction) and does not require to be specificity implemented.

The calculations were carried out with LAMMPS, a molecular dynamics software package that also accounts for other particle methods, such as SPH. The reader is referred to [34,35] for additional details on the numerical formulations and schemes used in the simulation of, respectively, the structure and the fluid.

The model does not account for temperature changes. However, this can be easily implemented in DMP [18].

2.2. Geometry

The starting geometry in the simulations was a three-dimensional single liquid core capsule with a diameter of 0.031 mm. As the purpose of this simulation was to simulate compression of single particles between two parallel plates, the drivers were defined as rectangular geometries that apply force to the capsule. The parallel plates were modelled with solid particles (Figure 3). The lower plate was stationary, while the upper plate moved as a rigid body under the effect of an applied force that compressed the capsules during the compression test.

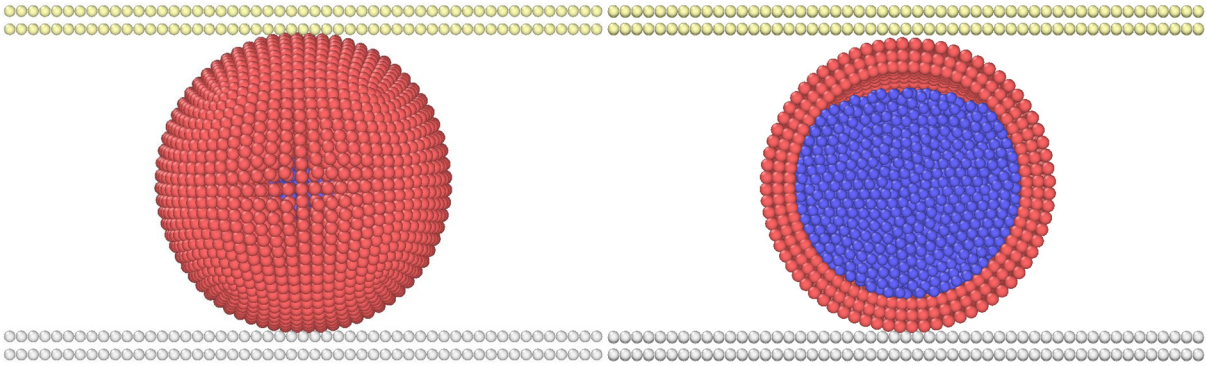

Figure 3. Initial simulation geometry.

Figure 3 shows the geometry of the shell and the parallel plates at the beginning of the simulation. A transversal cut of the capsule shows the fluid particles inside the capsule. In order to prevent penetration, repulsive forces were used between the fluid and the shell, the fluid and the plates, and the shell and the plates by applying no-penetration and no-slip boundary conditions, as explained in the previous section. The shell was built with three particle layers. Simulations with additional layers (i.e., more particles) were carried out and show similar results. In this study, we only considered elastic capsules. Viscoelastic can be modelled by implementing the method proposed in [36]. From Figure 3, it can be appreciated that the shell was not completely filled with fluid. The empty space was created by the small deformation of the capsule due to gravity and the resulting settling of the fluid particles. In theory, it is possible to add more particles to replenish the capsule. However, we decided not to do this, since the same phenomenon can also occur in real particles. This space is normally within 1%–2% of the total volume. We verified that within this range, and the results were not affected.

2.3. Main Simulation Parameters

The parameters used in the simulations can be divided into three groups (i.e., SPH, MSM, and boundaries) and are shown in Table 1.

The parameter that determines the elastic behaviour of the model is k_b, the Hookean coefficient of the computational springs. The actual Young's modulus of the capsules can be calculated from compression experiments with the technique proposed by Yap et al. [37]. In our case, it corresponds to E = 4.85 MPa. Once the Young's modulus is known, the value of k_b can be calculated with the following equation [38]:

$$k_b = \frac{6Et_0}{3n\sqrt{3}} \tag{13}$$

where E is the Young's modulus, t_0 is the thickness of the shell of the capsule, and n is the number of layers of the shell. The timestep used in the simulation was $\Delta t = 1 \times 10^{-10}$ s. We carried out a sensitivity analysis of the results with the timestep to make sure the results were independent of the timestep adopted.

The parallel plates applied a progressive pressure to the capsule until the capsule broke, replicating the experimental conditions. From the simulations, therefore, we can plot the force–displacement data and, for validation purposes, compare the plot with that obtained from the experiments.

2.4. Parametric Study and Influence of k_b and r_{max}

The capsule's deformability and strength are governed by two parameters: the Hookean coefficient of the computational springs (k_b) and the maximum distance between solid particles after which the computational spring breaks (r_{max}). In order to analyse the influence of these parameters on the deformability, strength, and type of fracture of the capsule, the main simulation, fitted to the experimental force–displacement curve, was

assessed in 9 different simulations modifying k_b (1.56, 4.67, and 14 N m^{-1}) and r_{max} (1.03·r_0, 1.2·r_0, and 1.27·r_0) values. Many other authors have applied similar methodologies in order to perform sensitivity analysis in different fields [39–42].

3. Results and Discussion

3.1. Validation of the Simulation of Capsule Compression between Two Parallel Plates

A parallel compression test of a single core–shell capsule under compressive load was reproduced in the simulations. The force–displacement curve obtained from these simulations was compared to the corresponding data obtained experimentally [25] for a core–shell with the same size and internal structure. For validation purposes, we compared the results with only one type of capsule available in the literature [25]. However, it must be noted that the parameters k_b describing the mechanical properties of the capsule are calculated by first-principles Equation (13), and are is not the result of fitting a free parameter to the experimental data.

In order to determine the optimal resolution of the core–shell model, various simulations with an increasing number of computational particles were compared. Each simulation had a different layer used to model the shell. The best compromise between accuracy and computational times was found with three layers. Figure 4 compares the force–displacement curve obtained with the model and with the experiments. Furthermore, an additional simulation with the capsule without fluid inside was carried out in order to understand the influence of the fluid on the capsule´s strength.

The results show that the compression can be divided into three regions: (i) an elastic region where the force is proportional to $\delta^{3/2}$ (where δ is the displacement), as predicted by Hertzian theory, and all of the load is supported by the external shell; (ii) an inelastic region where the stress reaches the fluid that adds additional resistance to the compression; (iii) a final region where the capsule breaks and collapses.

These three different stages were observed in both the experimental and the DMP force–displacement curves. The DMP results are very similar to the experimental results and reached the same maximal force required to break the capsule. The force–displacement curve from the simulation of the shell without fluid shows a completely different shape, which indicates that the internal fluid affects significantly the deformation of the capsule, especially at high deformations. It is important to highlight that the model does not account for plastic deformation. Locally, the rupture of every single bond was "fragile." However, this still produced a gradual rupture at the global level. In Figure 4, for instance, we defined the region before the rupture as "inelastic" because we did not observe capsule break-up. However, some of the bonds in the solid structure began to rupture, weakening the structure and producing the observed inelastic behaviour.

Figure 5 shows that the DMP model is consistent with the fracture and the capsule deformation for different coaxial load values applied during the compression test of the real capsule tested in the laboratory [25]. In order to save computational time, the resulting speed of the driver was higher in the simulations shown in Figure 5. However, quasi-static conditions were verified by carrying out simulations at different driver speeds, enabling a comparison between the force–displacement curves.

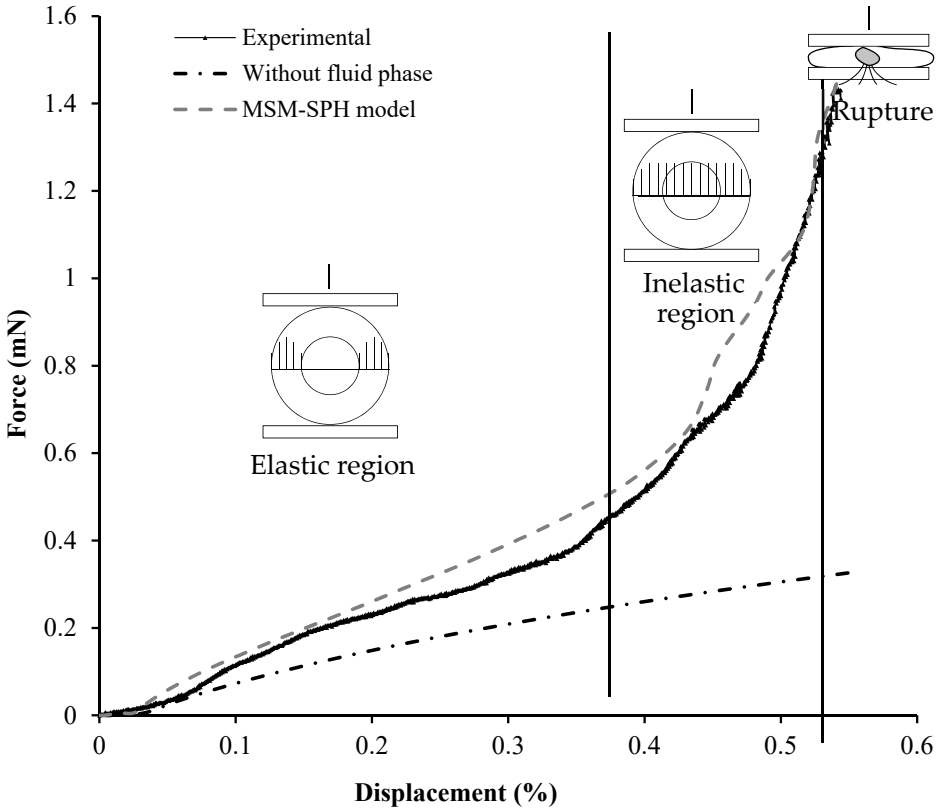

Figure 4. Force–displacement curve obtained from a laboratory parallel plate compression test for a single core–shell capsule, from a simulated single core–shell capsule without fluid inside and from a simulated single core–shell capsule. The upper plate displacement was expressed in %, taking into consideration the initial *y*-axis dimension of the capsule.

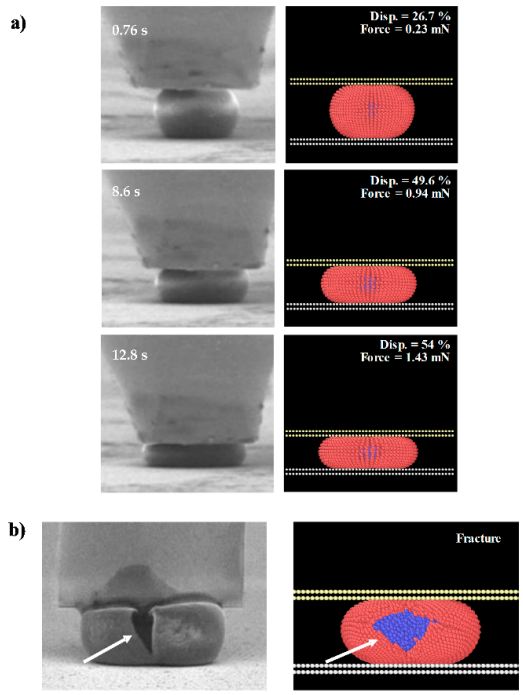

Figure 5. (**a**) Comparison between the deformation under coaxial load and (**b**) the fracture of a simulated elastic single liquid core–shell capsule by the Discrete Multi-Physics (DMP) approach and an elastic capsule of 16–50 μm being ruptured (from [43]).

3.2. Influence of the Fluid on the Capsule's Strength

Taking into consideration the previous results, it can be said that the internal liquid has an important effect on the force–displacement relationship.

Figure 6 shows an image sequence of the simulation of the parallel compression test of a single liquid core–shell capsule. Figure 6a shows the pressure of the internal fluid at the beginning of the test. As the capsule was compressed by the upper plate load and deformed, the pressure increased due to the load applied by the upper plate (Figure 6b,c). Finally, when the capsule started to break, the pressure of the fluid inside the capsule reduced because of the fluid released through the broken shell (Figure 6d).

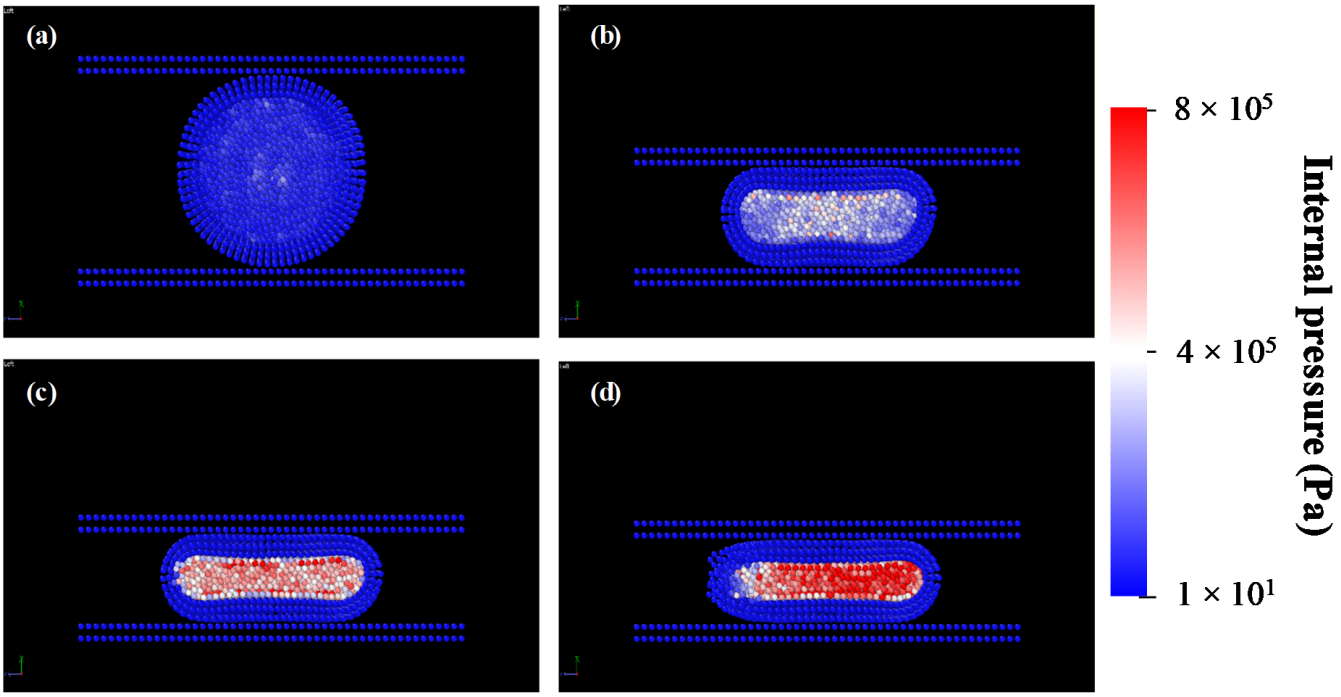

Figure 6. Simulation sequence of the parallel compression test of a single liquid core–shell capsule at different stages: (**a**) beginning of the simulation, (**b**) high deformation and slight increment of internal pressure, (**c**) slight deformation and significant increment of internal pressure and (**d**) fracture of the capsule.

3.3. Deformability and Strength of the Capsule (a Parametric Study)

In this section, a parametric study was carried out to understand how the behaviour of the capsule is affected by its mechanical properties: in particular, by k_b (which is related to the Young's modulus by Equation (13) and r_{max} (which provides the maximal local displacement before rupture). We studied three values of k_b (i.e., 14, 4.7, and 1.6 N m^{-1}) and r_{max} (i.e., 1.03·r_0, 1.2·r_0, and 1.27·r_0), and all nine possible pairings of these parameters.

Lower r_{max} values imply that the distances required to break the computational springs are shorter. This can be seen, for instance, in Figure 7b. Given the same k_b, the capsule broke when the displacement reached 45% for r_{max} = 1.03·r_0 and 54% for r_{max} = 1.2·r_0. The load that initiated the breakage of the capsule was also lower (0.54 versus 1.46 mN). This effect was observed for all three values of k_b, but it was more evident at high values of k_b.

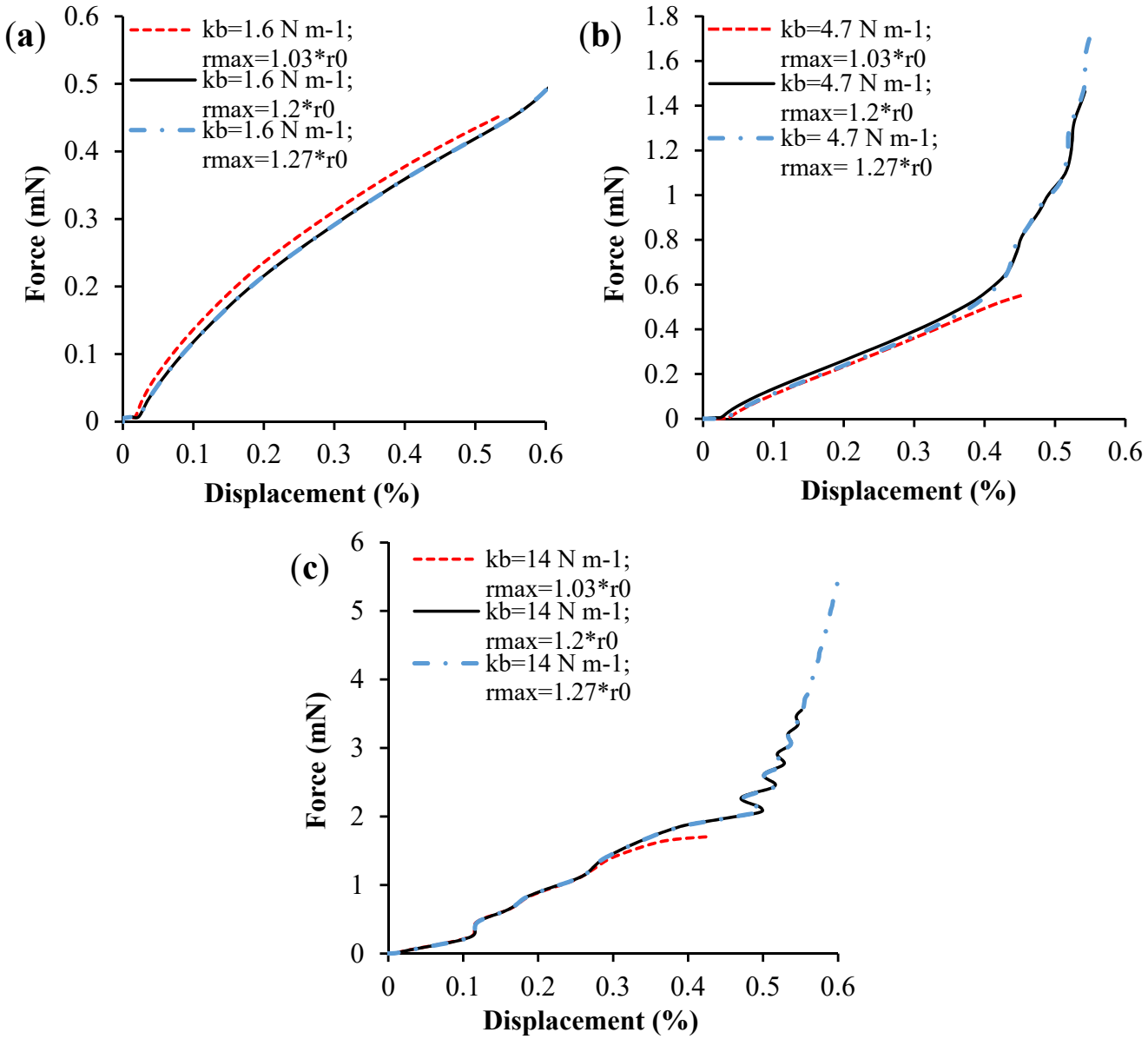

Figure 7. Simulated force–displacement curves for (**a**) k_b = 1.6 N^{-1} m and a range of r_{max} values, (**b**) k_b = 4.7 N^{-1} m and different values of r_{max} and (**c**) k_b = 1.6 N^{-1} m and different values of r_{max}.

As Figures 7 and 8 show, lower values of r_{max} mean that the local deformations required to break a computational bond are lower. As a result of this, breakage occurred at lower displacements in the simulations where r_{max} was lower. High values of k_b mean high Young's moduli (see Equation (13)). The shell was more rigid and, when it broke, the fracture started at a single location and propagated from there, forming a single wedge-shaped gash. When k_b was low, the capsule was flexible and showed little resistance to compression. In this case, the capsule tended to break at various locations at the same time during compression.

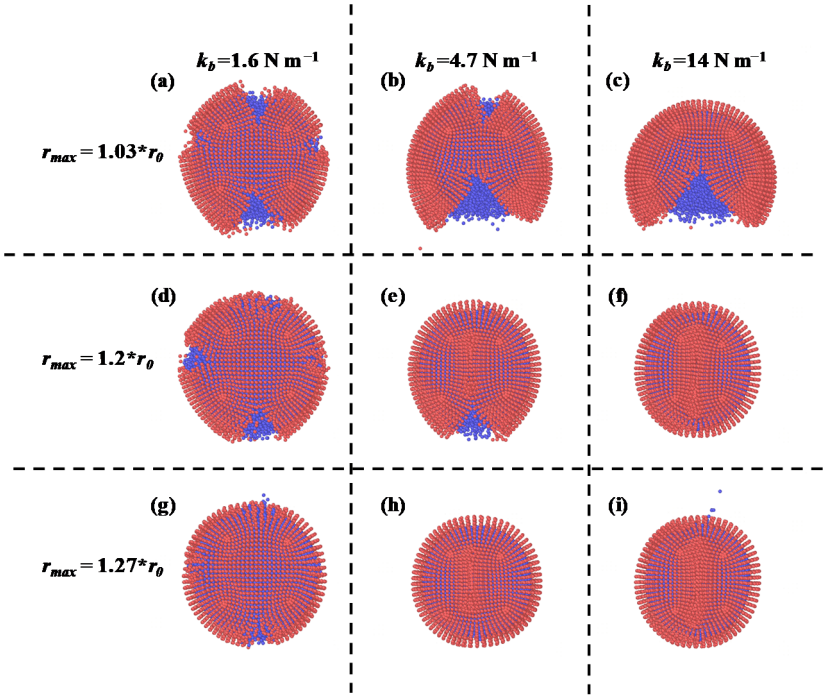

Figure 8. Capsule fractures (view from the top) at the end of each simulation for (**a**) k_b =1.6 N m^{-1} and r_{max} = 1.03 * r$_0$; (**b**) k_b =4.7 N m^{-1} and r_{max} = 1.03 * r$_0$; (**c**) k_b = 14 N m^{-1} and r_{max} = 1.03 * r$_0$; (**d**) k_b = 1.6 N m^{-1} and r_{max} = 1.2 * r$_0$; (**e**) k_b =4.7 N m^{-1} and r_{max} = 1.2 * r$_0$; (**f**) k_b = 14 N m^{-1} and r_{max} = 1.2 * r$_0$; (**g**) k_b = 1.6 N m^{-1} and r_{max} = 1.27 * r$_0$; (**h**) k_b = 4.7 N m^{-1} and r_{max} = 1.27 * r$_0$; (**i**) k_b = 14 N m^{-1} and r_{max} = 1.27 * r$_0$;

4. Conclusions

This study proposed a Discrete Multi-Physics model to simulate capsules formed by a shell containing a fluid. The liquid core was implemented with Smoothed Particle Hydrodynamics and the solid shell with the Lattice Spring Model.

The model was validated against experimental compression of a single core–shell capsule between two parallel plates. The results showed that the model replicates with good accuracy the behaviour of the real capsule. Three different stages were highlighted in the force–displacement curve occurring during the compression. In the first stage, the load was supported by the external shell and the behaviour was Hertzian (i.e., the force was proportional to $\delta^{3/2}$). During the second stage, the stress reached the fluid, which added additional resistance to the compression. Finally, in the third stage, the capsule broke and collapsed.

After the model had been validated, we carried out a parametric study that showed how the breakage of the capsule depended on its material properties. By changing the material properties, we varied (i) the maximal stress the capsule can resist before breaking, and (ii) the mode of breakage. In some cases, the shell cracked at one point that opened a wide gash in the capsule. In other cases, the shell fractured at multiple locations. This affected the way the liquid was released from the capsule. In the first scenario, the release was not uniform and was concentrated at one side of the capsule. In the second, the liquid was released from multiple points distributed around the capsule.

The proposed model can help the design of capsules with specific features. For instance, we can adjust the mechanical properties of the capsule to make sure that it breaks only when a precise stress level is reached. The model also simulates the liquid release occurring after breakage. In this way, we can design the capsule to make sure that the liquid is released effectively. In fact, the capsule breaks in different ways according to its mechanical properties, and only specific combinations of these properties allow for a uniform release of the liquid after breakage.

Author Contributions: Conceptualization, I.N.R.-R., A.A., Z.Z. and A.G.H.; Methodology, I.N.R.-R. and A.A.; Software, I.N.R.-R. and A.A.; Validation, I.N.R.-R., A.A. and Z.Z.; Formal analysis, I.N.R.-R. and A.A.; Investigation, I.N.R.-R. and A.A.; Data curation, I.N.R.-R.; Writing—original draft preparation, I.N.R.-R.; Writing—review and editing, I.N.R.-R., A.A., Z.Z. and A.G.H.; Project administration, I.N.R.-R. and A.G.H.; Supervision, A.G.H. and A.A.; Project administration, I.N.R.-R. and A.G.H.; Funding acquisition, A.G.H. All authors have read and agreed to the published version of the manuscript.

Funding: This research received funding from the European Union's H2020 Programme for research, technological development, and demonstration under grant agreement number 721493.

Institutional Review Board Statement: Not applicable.

Informed Consent Statement: Not applicable.

Data Availability Statement: The data presented in this study are available on request from the corresponding author.

Acknowledgments: The research presented in this paper was carried out as part of the H2020-MSCA-ETN-2016.

Conflicts of Interest: The authors declare no conflict of interest.

References

1. Trojanowska, A.; Nogalska, A.; Garcia, R.; Giamberini, M.; Tylkowski, B. Technological Solutions for Encapsulation. *J. Magn. Magn. Mater.* **2017**, *2*, 1–20.
2. Martins, E.; Poncelet, D.; Rodrigues, R.C.; Renard, D. Oil Encapsulation Techniques Using Alginate as Encapsulating Agent: Applications and Drawbacks. *J. Microencapsul.* **2017**, *34*, 754–771. [CrossRef]
3. Thuong, N.P.; Thanh, V.T.; Cang, M.H.; Lam, T.D.; Huong, N.C.; Hong Nhan, L.T.; Truc, T.T.; Tran, Q.T.; Bach, L.G. Microencapsulation of Lemongrass (Cymbopogon Citratus) Essential Oil via Spray Drying: Effects of Feed Emulsion Parameters. *Processes* **2020**, *8*, 40. [CrossRef]
4. O'Sullivan, M.; Zhang, Z.; Vincent, B. Silica-Shell/Oil-Core Microcapsules with Controlled Shell Thickness and Their Breakage Stress. *Langmuir* **2009**, *25*, 7962–7966. [CrossRef]
5. Norambuena-contreras, J.; Yalcin, E.; Garcia, A.; Al-mansoori, T.; Yilmaz, M.; Hudson-griffiths, R. Effect of Mixing and Ageing on the Mechanical and Self-Healing Properties of Asphalt Mixtures Containing Polymeric Capsules. *Constr. Build. Mater.* **2018**, *175*, 254–266. [CrossRef]
6. Zhu, D.Y.; Rong, M.Z.; Zhang, M.Q. Self-Healing Polymeric Materials Based on Microencapsulated Healing Agents: From Design to Preparation. *Prog. Polym. Sci.* **2015**, *49–50*, 175–220. [CrossRef]
7. Casanova, F.; Santos, L. Encapsulation of Cosmetic Active Ingredients for Topical Application-a Review. *J. Microencapsul.* **2016**, *33*, 1–17. [CrossRef]
8. Tsai, F.H.; Chiang, P.Y.; Kitamura, Y.; Kokawa, M.; Islam, M.Z. Producing Liquid-Core Hydrogel Beads by Reverse Spherification: Effect of Secondary Gelation on Physical Properties and Release Characteristics. *Food Hydrocoll.* **2017**, *62*, 140–148. [CrossRef]
9. Stan, M.S.; Chirila, L.; Popescu, A.; Radulescu, D.M.; Radulescu, D.E.; Dinischiotu, A. Essential Oil Microcapsules Immobilized on Textiles and Certain Induced Effects. *Materials* **2019**, *12*, 2029. [CrossRef]
10. Rodríguez-Dorado, R.; Landín, M.; Altai, A.; Russo, P.; Aquino, R.P.; Del Gaudio, P. A Novel Method for the Production of Core-Shell Microparticles by Inverse Gelation Optimized with Artificial Intelligent Tools. *Int. J. Pharm.* **2018**, *538*, 97–104. [CrossRef]
11. Sheng, W.; Li, W.; Li, B.; Li, C.; Xu, Y.; Guo, X.; Zhou, F.; Jia, X. Mussel-Inspired Photografting on Colloidal Spheres: A Generalized Self-Template Route to Stimuli-Responsive Hollow Spheres for Controlled Pesticide Release. *Macromol. Rapid Commun.* **2015**, *36*, 1640–1645. [CrossRef]
12. Huang, H.; Ye, G.; Qian, C.; Schlangen, E. Self-Healing in Cementitious Materials: Materials, Methods and Service Conditions. *Mater. Des.* **2016**, *92*, 499–511. [CrossRef]
13. García, Á.; Schlangen, E.; Van De Ven, M. Properties of Capsules Containing Rejuvenators for Their Use in Asphalt Concrete. *Fuel* **2011**, *90*, 583–591. [CrossRef]
14. Al-Mansoori, T.; Norambuena-Contreras, J.; Micaelo, R.; Garcia, A. Self-Healing of Asphalt Mastic by the Action of Polymeric Capsules Containing Rejuvenators. *Constr. Build. Mater.* **2018**, *161*, 330–339. [CrossRef]
15. Mercadé-Prieto, R.; Zhang, Z. Mechanical Characterization of Microspheres Capsules, Cells and Beads: A Review. *J. Microencapsul.* **2012**, *29*, 277–285. [CrossRef] [PubMed]
16. Walter, J.; Salsac, A.V.; Barthes-Biesel, D.; Le Tallec, P. Coupling of Finite Element and Boundary Integral Methods for a Capsule in a Stokes Flow. *Int. J. Numer. Methods Eng.* **2010**, *83*, 829–850. [CrossRef]
17. Müller, M.; Schirm, S.; Teschner, M.; Heidelberger, B.; Gross, M. Interaction of Fluids with Deformable Solids. *Comput. Animat. Virtual Worlds* **2004**, *15*, 159–171. [CrossRef]

18. Alexiadis, A. The Discrete Multi-Hybrid System for the Simulation of Solid-Liquid Flows. *PLoS ONE* **2015**, *10*, e0124678. [CrossRef]
19. Ariane, M.; Wen, W.; Vigolo, D.; Brill, A.; Nash, F.G.B.; Barigou, M.; Alexiadis, A. Modelling and Simulation of Flow and Agglomeration in Deep Veins Valves Using Discrete Multi Physics. *Comput. Biol. Med.* **2017**, *89*, 96–103. [CrossRef]
20. Alexiadis, A.; Stamatopoulos, K.; Wen, W.; Batchelor, H.K.; Bakalis, S.; Barigou, M.; Simmons, M.J.H. Using Discrete Multi-Physics for Detailed Exploration of Hydrodynamics in an in Vitro Colon System. *Comput. Biol. Med.* **2017**, *81*, 188–198. [CrossRef]
21. Ariane, M.; Kassinos, S.; Velaga, S.; Alexiadis, A. Discrete Multi-Physics Simulations of Diffusive and Convective Mass Transfer in Boundary Layers Containing Motile Cilia in Lungs. *Comput. Biol. Med.* **2018**, *95*, 34–42. [CrossRef]
22. Ariane, M.; Vigolo, D.; Brill, A.; Nash, F.G.B.; Barigou, M.; Alexiadis, A. Using Discrete Multi-Physics for Studying the Dynamics of Emboli in Flexible Venous Valves. *Comput. Fluids* **2018**, *166*, 57–63. [CrossRef]
23. Alexiadis, A.; Ghraybeh, S.; Qiao, G. Natural Convection and Solidification of Phase-Change Materials in Circular Pipes: A SPH Approach. *Comput. Mater. Sci.* **2018**, *150*, 475–483. [CrossRef]
24. Rahmat, A.; Barigou, M.; Alexiadis, A. Deformation and Rupture of Compound Cells under Shear: A Discrete Multiphysics Study. *Phys. Fluids* **2019**, *31*. [CrossRef]
25. Mercadé-Prieto, R.; Nguyen, B.; Allen, R.; York, D.; Preece, J.A.; Goodwin, T.E.; Zhang, Z. Determination of the Elastic Properties of Single Microcapsules Using Micromanipulation and Finite Element Modeling. *Chem. Eng. Sci.* **2011**, *66*, 2042–2049. [CrossRef]
26. Gray, A.; Egan, S.; Bakalis, S.; Zhang, Z. Determination of Microcapsule Physicochemical, Structural, and Mechanical Properties. *Particuology* **2016**, *24*, 32–43. [CrossRef]
27. Monaghan, J.J. Smoothed Particle Hydrodynamics. *Rep. Prog. Phys.* **2005**, *68*, 1703–1759. [CrossRef]
28. Huang, Y.J.; Nydal, O.J. Coupling of Discrete-Element Method and Smoothed Particle Hydrodynamics for Liquid-Solid Flows. *Theor. Appl. Mech. Lett.* **2012**, *2*, 012002. [CrossRef]
29. Lucy, L.B. A Numerical Approach to the Testing of the Fission Hypothesis. *Astron. J.* **1977**, *82*, 1013–1024. [CrossRef]
30. Morris, J.P.; Fox, P.J.; Zhu, Y. Modeling Low Reynolds Number Incompressible Flows Using SPH. *Int. J. Numer. Methods Fluids* **1997**, *136*, 214–226. [CrossRef]
31. Cole, R.H. *Underwater Explosions*; Pinceton University Press: Pinceton, NJ, USA, 1948.
32. Kot, M.; Nagahashi, H.; Szymczak, P. Elastic Moduli of Simple Mass Spring Models. *Vis. Comput.* **2015**, *31*, 1339–1350. [CrossRef]
33. Alexiadis, A. A New Framework for Modelling the Dynamics and the Breakage of Capsules, Vesicles and Cells in Fluid Flow. *Procedia IUTAM* **2015**, *16*, 80–88. [CrossRef]
34. Plimpton, S. Fast Parallel Algorithms for Short-Range Molecular Dynamics. *J. Comput. Phys.* **1995**, *117*, 1–19. [CrossRef]
35. Ganzenm, G.C.; Steinhauser, M.O.; Van Liedekerke, P. The Implementation of Smooth Particle Hydrodynamics in LAMMPS. 2011; pp. 1–23. Available online: https://lammps.sandia.gov/doc/PDF/SPH_LAMMPS_userguide.pdf (accessed on 10 December 2018).
36. Sahputra, I.H.; Alexiadis, A.; Adams, M.J. A Coarse Grained Model for Viscoelastic Solids in Discrete Multiphysics Simulations. *ChemEngineering* **2020**, *4*, 30. [CrossRef]
37. Yap, S.F.; Adams, M.J.; Seville, J.P.K.; Zhang, Z. Single and Bulk Compression of Pharmaceutical Excipients: Evaluation of Mechanical Properties. *Powder Technol.* **2008**, *185*, 1–10. [CrossRef]
38. Van Liedekerke, P.; Tijskens, E.; Ramon, H.; Ghysels, P.; Samaey, G.; Roose, D. Particle-Based Model to Simulate the Micromechanics of Biological Cells. *Phys. Rev. E Stat. Nonlinear Soft Matter Phys.* **2010**, *81*, 1–15. [CrossRef]
39. Ghasemi, H.; Darjani, S.; Mazloomi, H.; Mozaffari, S. Preparation of Stable Multiple Emulsions Using Food-Grade Emulsifiers: Evaluating the Effects of Emulsifier Concentration, W/O Phase Ratio, and Emulsification Process. *SN Appl. Sci.* **2020**, *2*. [CrossRef]
40. Ghasemi, H.; Aghabarari, B.; Alizadeh, M.; Khanlarkhani, A.; Abu-Zahra, N. High Efficiency Decolorization of Wastewater by Fenton Catalyst: Magnetic Iron-Copper Hybrid Oxides. *J. Water Process Eng.* **2020**, *37*, 101540. [CrossRef]
41. Sokolov, A.; Mozaffari, A.; Zhang, R.; De Pablo, J.J.; Snezhko, A. Emergence of Radial Tree of Bend Stripes in Active Nematics. *Phys. Rev. X* **2019**, *9*, 31014. [CrossRef]
42. Li, J.; Dong, S.; Hua, W.; Li, X.; Pan, X. Numerical Investigation of Hydraulic Fracture Propagation Based on Cohesive Zone Model in Naturally Fractured Formations. *Processes* **2019**, *7*, 28. [CrossRef]
43. Ren, Y.L.; Donald, A.M.; Zhang, Z.B. Investigation of Radiation Damage to Microcapsules in Environmental SEM. *Mater. Sci. Technol.* **2007**, *23*, 857–864. [CrossRef]